LETTERS

# Chemical identification of individual surface atoms by atomic force microscopy

Yoshiaki Sugimoto[1], Pablo Pou[2], Masayuki Abe[1,3], Pavel Jelinek[4], Rubén Pérez[2], Seizo Morita[1] & Óscar Custance[1]

**Scanning probe microscopy is a versatile and powerful method that uses sharp tips to image, measure and manipulate matter at surfaces with atomic resolution[1,2]. At cryogenic temperatures, scanning probe microscopy can even provide electron tunnelling spectra that serve as fingerprints of the vibrational properties of adsorbed molecules[3–5] and of the electronic properties of magnetic impurity atoms[6,7], thereby allowing chemical identification. But in many instances, and particularly for insulating systems, determining the exact chemical composition of surfaces or nanostructures remains a considerable challenge. In principle, dynamic force microscopy should make it possible to overcome this problem: it can image insulator, semiconductor and metal surfaces with true atomic resolution[8–10], by detecting and precisely measuring[11–13] the short-range forces that arise with the onset of chemical bonding between the tip and surface atoms[14,15] and that depend sensitively on the chemical identity of the atoms involved. Here we report precise measurements of such short-range chemical forces, and show that their dependence on the force microscope tip used can be overcome through a normalization procedure. This allows us to use the chemical force measurements as the basis for atomic recognition, even at room temperature. We illustrate the performance of this approach by imaging the surface of a particularly challenging alloy system and successfully identifying the three constituent atomic species silicon, tin and lead, even though these exhibit very similar chemical properties and identical surface position preferences that render any discrimination attempt based on topographic measurements impossible.**

The chemical identification of single atoms and molecules at surfaces has been pursued since the invention of both the scanning tunnelling microscope and the atomic force microscope (AFM). Particularly promising in this quest is dynamic force microscopy, which achieves true atomic imaging resolution[8–10] by detecting the short-range forces associated with the onset of the chemical bond between the outermost atom of the tip apex and the surface atoms being imaged[14,15] (see Fig. 1 for schematic illustration of the method and imaging examples). Moreover, dynamic force spectroscopy[11–13] makes it possible to quantify these forces.

Figure 2a shows five sets of dynamic force spectra measured on a single atomic layer of Sn grown on a Si(111) substrate. Each set of force curves was obtained over an Sn atom and an Si atom having the same local surface configuration as the corresponding atoms highlighted in the topographic image shown in Fig. 1d, always using identical acquisition and analysis protocols (see Methods). However, the sets were collected over multiple measurement sessions, using tips that had different apex terminations. These tip apexes presumably differ in both structure and composition (Sn or Si), as sometimes slight tip–surface contacts were intentionally produced before the acquisition of each set of force curves. The sets seem to share only one feature: curves measured over the Si atoms are characterized by a stronger attractive interaction force. Given the high degree of stability, lateral positioning accuracy, and reproducibility provided by our acquisition protocol[12,16], we attribute the variability seen in the data in Fig. 2a to a strong tip dependence of both the registered

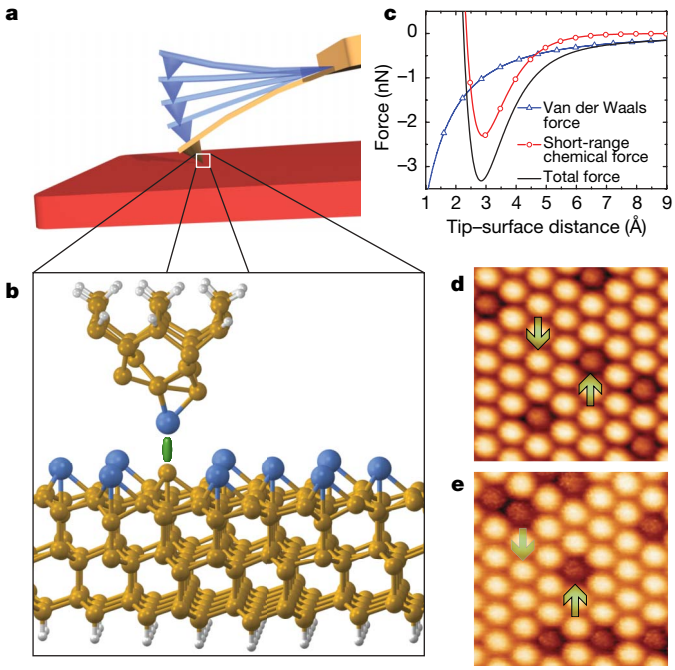


**Figure 1 | Dynamic force microscopy with atomic resolution.** Schematic illustration of AFM operation in dynamic mode (**a**), and of the onset of the chemical bonding between the outermost tip atom and a surface atom (highlighted by the green stick) that gives rise to the atomic contrast[14,15] (**b**). However, the tip experiences not only the short-range force associated with this chemical interaction, but also long-range force contributions that arise from van der Waals and electrostatic interactions between tip and surface (though the effect of the latter is usually minimized through appropriate choice of the experimental set-up). **c**, Curves obtained with analytical expressions for the van der Waals force, the short-range chemical interaction force, and the total force to illustrate their dependence on the absolute tip–surface distance. **d**–**e**, Dynamic force microscopy topographic images of a single-atomic layer of Sn (**d**) and Pb (**e**) grown, respectively, over a Si(111) substrate. At these surfaces, a small concentration of substitutional Si defects, characterized by a diminished topographic contrast[20], is usually found. The green arrows indicate atomic positions where force spectroscopic measurements were performed (see Fig. 2). Image dimensions are $(4.3 \times 4.3)$ nm$^2$; for the acquisition parameters see the Supplementary Information.

[1]Graduate School of Engineering, Osaka University, 2-1 Yamada-Oka, 565-0871 Suita, Osaka, Japan. [2]Departamento de Física Teórica de la Materia Condensada, Universidad Autónoma de Madrid, 28049 Madrid, Spain. [3]PRESTO, Japan Science and Technology Agency, Saitama 332-0012, Japan. [4]Institute of Physics, Academy of Sciences of the Czech Republic, Cukrovarnická 10, 1862 53, Prague, Czech Republic.

maximum attractive force value and the distance dependence of the attractive and repulsive regions of the curves.

A meaningful comparison of measured short-range forces requires some data processing to reduce the variability caused by the use of tips with different terminations. We have found that the relative interaction ratio, that is, the ratio of the maximum attractive short-range forces of the two curves within a set of measurements over Si and Sn (acquired using a tip that had the same apex termination), remains nearly constant. This is illustrated in Fig. 2b, where each curve within a given measurement set has been normalized to the absolute value of the maximum attractive short-range force of the Si curve of that set ($|F_{Si(set)}|$). The normalization reveals an average value for the relative interaction ratio of $0.77 \pm 0.02$. This approach has also been validated for elements such as Pb or In in similar surfaces (see Fig. 1e, Fig. 2c, d and Supplementary Information). Using the same acquisition and analysis protocols as applied when studying the mixed Sn/Si surface layer, several sets of short-range force curves were obtained over structurally equivalent atoms (for the Pb/Si layer, these are highlighted by arrows in Fig. 1e). The data revealed an average relative interaction ratio of $0.59 \pm 0.03$ for Pb and Si in the Pb-terminated surface (Fig. 2c, d), and an average relative interaction ratio for In and Si of $0.72 \pm 0.04$ in the In-terminated one.

To corroborate the experimental observations, we conducted large-scale first-principles calculations (see Methods) using atomically extended nanometre-scale asperities[17] as tip-apex models. In these calculations, homogeneous tip apexes that have different structures for probing the Sn and Si atoms of a model of the mixed Sn/Si surface layer (shown in Fig. 1b) produce different short-range force curves (Fig. 2e). If the tip apexes have the same termination structure but a different element at the outermost position, we obtain weaker short-range forces for Sn-terminated tips than for Si-terminated tips (Fig. 2e). In all these cases, as in the experiments, the tip–surface interaction is stronger over Si surface atoms than over Sn atoms (Fig. 2e). But independently of tip-apex structure and the chemical termination of the tips, the relative interaction ratios of the maximum attractive forces calculated over the Sn and Si atoms for a given tip are all similar, with an average value of $0.71 \pm 0.07$ (Fig. 2f) that is close to the experimental ratio.

To gain some insight into the behaviour of the short-range forces, we have developed a simple analytical model that assumes that tip and sample deform elastically in response to the short-range chemical interaction between the tip apex and the closest surface atoms (P.P., Y.S., P.J., M.A., S.M., O.C. and R.P., manuscript in preparation). The model indicates that although the shape of the force-versus-distance curves depends on the elastic response of the system, the value of the maximum attractive short-range force is determined only by the short-range chemical interaction (data not shown). The minimum short-range force value registered for a given surface atom (corresponding to maximum attractive force) is thus expected to depend significantly on the chemical composition and structure of the tip apex (an effect seen in the data in Fig. 2e), and will also depend on the relative orientation of the tip with respect to the surface[18,19]. These three factors explain the strong tip dependence found in the experiments (see Fig. 2a and c). However, when the relative interaction ratio of the maximum attractive short-range forces for two atomic species probed with the same tip is considered, the common features associated with the structural characteristics of the tip-apex cancel out, and the intrinsic strength of the chemical bonding interaction between the outermost tip atom and the closest surface atom is revealed (Fig. 2b, d and f). This explanation can be rationalized for semiconductor surfaces using accepted combination rules for covalent chemical interactions; it can, in fact, be generalized to multi-element systems by considering that when individually probing the atoms of such systems with a given tip apex, interactions between pairs of atomic species are obtained. This ensures that the relative strengths of the minimum short-range forces are almost independent from the tip-apex structure or chemical termination (see Supplementary Information for further details).

By determining the ratio of the maximum attractive short-range forces as outlined above, it is possible to identify individual atoms in

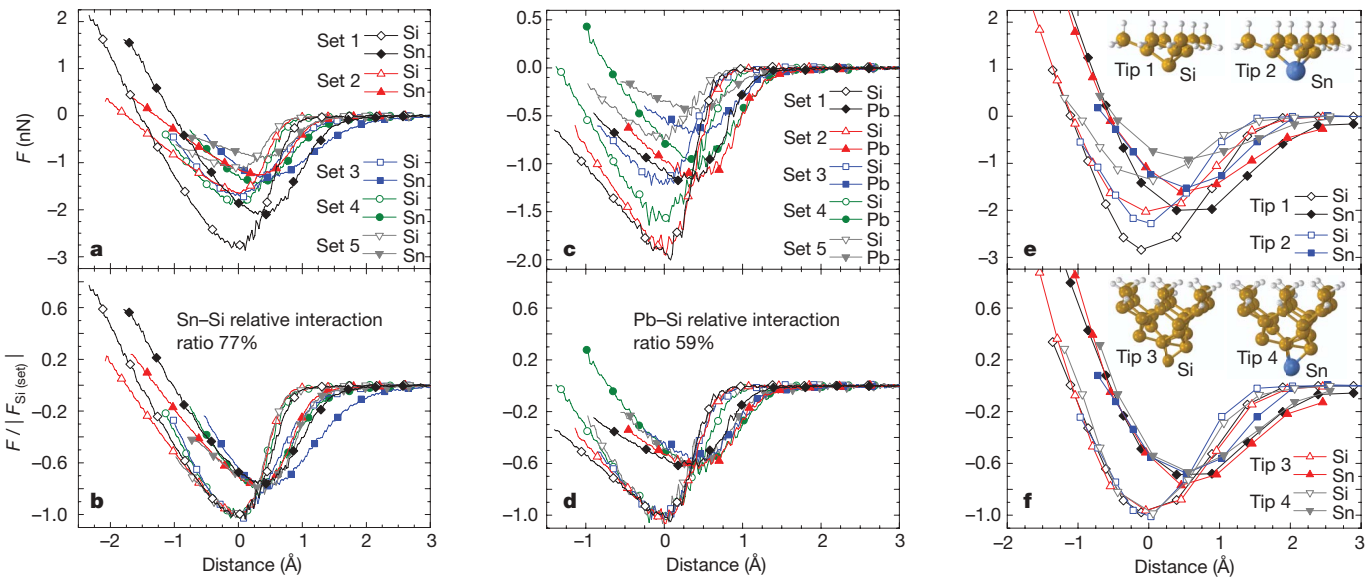


**Figure 2 | Probing short-range chemical interaction forces. a**, Sets of short-range force curves obtained over structurally equivalent Sn and Si atoms. All curves are obtained using identical acquisition and analysis protocols, but the tips differ from set to set. **b**, The same force curves as in **a**, but the curves in each set are now normalized to the absolute value of the minimum short-range force of the Si curve ($|F_{Si(set)}|$). **c**, **d**, Sets of short-range force curves for Pb and Si, obtained in the same way as for Sn and Si, before (**c**) and after (**d**) normalization. The average relative interaction ratios calibrated against Si, or the maximum attractive short-range forces for Sn and Pb relative to those of Si (77% and 59%, respectively), provide an intrinsic signature for the chemical identification of individual atoms. Each experimental force characteristic shown here was obtained from the measurement of a hundred spectroscopic curves (see Methods for details). The acquisition parameters are available in the Supplementary Information. **e**, **f**, Chemical force curves calculated for different tip-apex models (see insets for structural and chemical characteristics) over the Sn and Si atoms of the $(\sqrt{3} \times \sqrt{3})$ R30° surface model shown in Fig. 1b. The curves are shown before (**e**) and after (**f**) normalization. In both the experimental and the calculated short-range force curves, the distance axes denote the tip–sample relative displacement (see Methods for details).

multi-element systems. This capability of the AFM is demonstrated in Fig. 3, where we have unambiguously discriminated between the three species—topographically not clearly distinguishable—of a surface alloy comprised of Si, Sn, and Pb atoms mixed in equal proportions

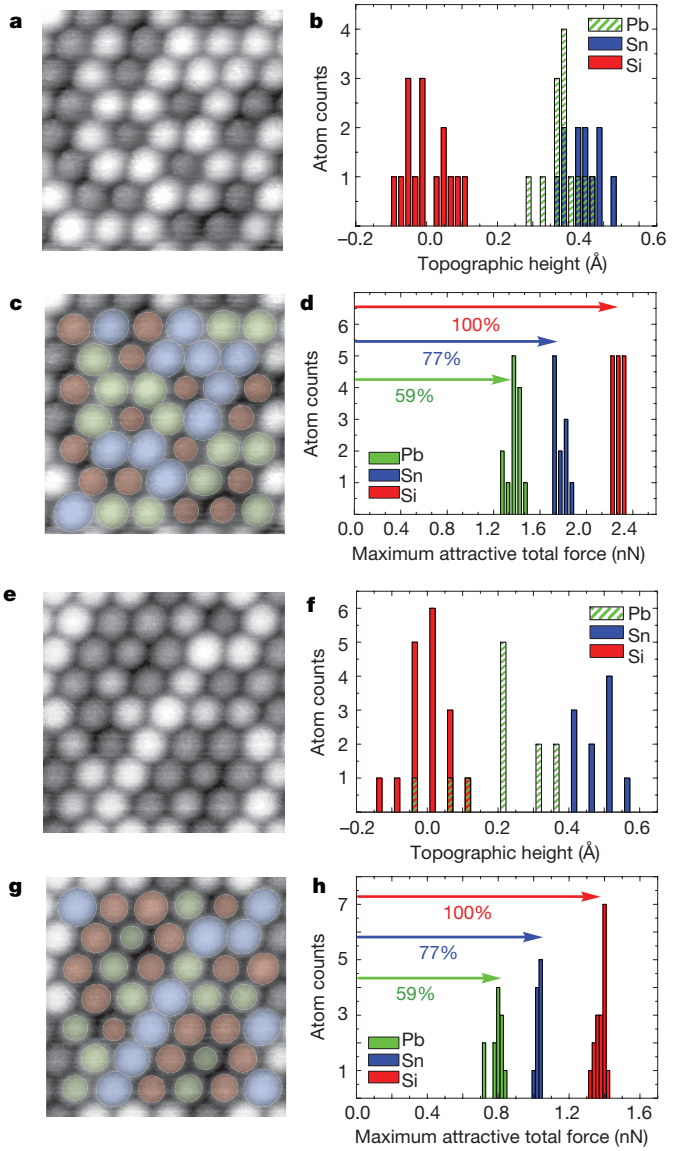


**Figure 3 | Single-atom chemical identification.** **a**, Topographic image of a surface alloy composed by Si, Sn and Pb atoms blended in equal proportions on a Si(111) substrate. **b**, Height distribution of the atoms in **a**, showing that Pb and Sn atoms with few nearest-neighbouring Si atoms appear indistinguishable in topography. **c**, Local chemical composition of the image in **a**. Blue, green, and red atoms correspond to Sn, Pb and Si, respectively. **d**, Distribution of maximum attractive total forces measured over the atoms in **a**. By using the relative interaction ratio determined for Sn/Si and Pb/Si (Fig. 2b and d), each of the three groups of forces can be attributed to interactions measured over Sn, Pb and Si atoms. **e**, Topographic image similar to that in **a**, but showing a region where some Pb atoms are almost completely surrounded by Si atoms. These Pb atoms (identified in **g** by a darker shade of green) are indistinguishable from the surrounding Si atoms, as illustrated by the topographic height distribution histogram (**f**). The local chemical composition, shown in **g**, can still be unambiguously assigned by measuring the total force values over each surface atom and using the relative interaction ratios for Sn/Si and Pb/Si to attribute the three groups of maximum attractive forces to interactions measured over Sn, Pb and Si atoms (**h**). The colour code for labelling the Pb, Sn and Si atoms in **g** is the same as in **c**. Image dimensions are (4. 3 × 4.3) nm$^2$. The images were acquired close to the onset of the short-range interaction[20]; for the acquisition parameters see the Supplementary Information.

(Fig. 3a and e). In this instance, we systematically recorded the total tip–surface interaction force over each atom seen in the images in Fig. 3a and e, respectively. The measured maximum attractive total forces were found to fall into three distinct groups (see histograms in Fig. 3d and h, respectively). When taking into account the relative interaction ratio for Sn and Si and for Pb and Si determined in our earlier experiments (Fig. 2b and d), these groups can be assigned to forces obtained over Sn, Pb and Si atoms (Fig. 3d and h) and hence the chemical identity of each surface atom can be determined (Fig. 3c and g). The significant discrepancy between the total force values in Fig. 3d and h—obtained in two separate measurement sessions using different tips—confirms that although tip characteristics strongly influence measured forces, they do not affect the ability to chemically identify surface atoms. These results also corroborate the robustness of the procedure, as the identification in Fig. 3 has been accomplished by using the maximum attractive total forces instead of the short-range forces. This more straightforward identification process, which avoids the non-trivial and time-consuming separation of the short- and long-range contributions to the total force[20], can be extended to other systems if the total force is not dominated by long-range interactions and there are no pronounced in-plane local spatial variations of the long-range forces. In the experiments shown in Fig. 3, for instance, the long-range contribution at the minimum positions was only 10% to 18% of the total interaction force (see the Supplementary Information).

We note that it would have been impossible to reveal the local atomic composition of these surface alloy regions using topographic information. For example, in areas with locally homogeneous distributions of Si atoms (Fig. 3a), Pb and Sn appear indistinguishable in topography; this is clearly illustrated by the atomic height distribution histogram (Fig. 3b). But in regions where Si atoms cluster together (Fig. 3e), any Pb atoms that are surrounded almost completely by Si atoms (differentiated from other Pb atoms in Fig. 3g by a darker shade of green) are indistinguishable from the Si atoms; again, this effect is clearly illustrated by the histogram shown in Fig. 3f. These topographic variations with the number of nearest-neighbouring Si atoms[20,21] have been attributed to a subtle coupling between charge transfer and atomic relaxations[22]. For closer tip–surface distances, relative variations in the atomic contrast—which would further hinder a topographic discrimination attempt—are expected owing to differences in the strength of the interaction forces over the atoms and tip-induced atomic relaxations[20]. Attempts to scan at tip–surface distances close to the maximum attractive forces—where the interaction between the outermost tip atom and a surface atom dominates the signal, and hence unambiguous chemical information of the atomic surface species can be obtained—result in most of the cases in unstable imaging, or even in modifications of the tip apex or surface due to strong tip–surface lateral forces.

The present approach to characterizing the local composition of a multi-element system at the atomic level, which is based on the detection of the short-range chemical forces between the outermost atom of an AFM tip and individual surface atoms, should be widely applicable. It does require prior calibration of the relative interaction ratio of the maximum attractive short-range forces between pairs of atomic species on a well-defined system; but once obtained, the ratios (which are practically independent of tip apex characteristics) can serve as fingerprints for chemical recognition in subsequent measurements. We believe that the chemical identification capabilities demonstrated here hold substantial promise for affecting research areas such as catalysis, materials science or semiconductor technology, in which important functional properties are controlled by the chemical nature and short-range ordering of individual atoms, defects, adsorbates or dopants.

## METHODS

**Dynamic force microscopy and spectroscopy measurements.** We used a home-built ultrahigh vacuum dynamic AFM powered by a commercial scanning probe controller (Dulcinea, Nanotec Electrónica, Madrid, Spain) and operated at room

temperature under the frequency modulation detection method[23]. The cantilever was instantaneously excited to its first mechanical resonant frequency keeping the oscillation amplitude constant. The main observable was the shift of the first mechanical resonant frequency ($\Delta f$) from the free-oscillation value upon the forces acting on the tip at the cantilever free end[24]. Force spectroscopy was performed recording the $\Delta f$ signal as a function of the tip–sample relative vertical displacement ($Z$). The determination of the corresponding cantilever stiffness and oscillation amplitude values is described elsewhere[12]. The absence of any tip or surface modification during the spectroscopic acquisition was carefully and properly checked[12]. During imaging, and for each spectroscopic measurement, the long-range electrostatic interaction was minimized by compensating the tip–surface contact potential difference. For the calibration of the relative interaction ratio in Fig. 2, we first performed the identification of Sn, Pb, and Si in the corresponding bi-atomic overlayers (Fig. 1d, e) by changing the relative concentration of the two elements[20].

In Fig. 2, a single spectroscopic measurement comprised the successive acquisition of a hundred equivalent $\Delta f(Z)$ curves over the topmost part of the surface atom with a lateral precision better than $\pm 0.1$ Å, provided by our atom-tracking implementation[12,16]. In each case, these $\Delta f(Z)$ curves were averaged in a single $\Delta f(Z)$ characteristic from which we obtained the total interaction force using the inversion procedure proposed by Sader and Jarvis[25]. For each set of curves, the compensation of the topographic effects on $Z$ associated with the spectroscopic acquisition[20] was then undertaken; this sets the separation distance between the two force minima and provides a common origin with respect to the surface plane[20]. The short-range chemical forces were obtained afterwards by the subtraction of an appropriate fit[11,12] over the long-range interaction region to the total force, where this long-range region is defined from the free oscillation to the $Z$ position at which both curves start splitting owing to the onset of the short-range interaction. For clarity in the representation, the origin of the $Z$ axis for each set was shifted to the position for the Si minimum (keeping the original separation between the minima constant), so that all the sets share the same distance origin when compared. In the case of the experiments shown in Fig. 3, only ten $\Delta f(Z)$ curves were measured over each atom. The surface alloy was prepared by the deposition of approximately one-sixth of a monolayer of Pb—one monolayer corresponds to the surface atomic density of a (111) plane of a Si crystal—and one-ninth of a monolayer of Sn over the Si(111)-$(7 \times 7)$ surface, followed by sample annealing at 700 K.

**First-principles calculations.** Calculations are based in density functional theory implemented with a local orbital basis using the FIREBALL code[26], which offers a very favourable accuracy-to-efficiency balance. The details of the minimal basis we used are described elsewhere[20]. To model the surface we considered a $(6 \times 6)$ periodic slab that includes six Si layers with H saturating the dangling bonds at the deeper layer (Fig. 1b). Only the $\Gamma$ point was included in the sampling of the Brillouin zone. The tip–surface interaction energy was determined in a stepwise, quasistatic manner by approaching the tip parallel to the surface. At each step, the atoms in the slab and the tip model were allowed to relax to their ground-state configuration with convergence criteria for the total energy and forces of $10^{-6}$ eV and 0.05 eV Å$^{-1}$. Only the H-saturated atoms at the topmost part of the tip models (Fig. 2e and f) and the Si and H layers at the bottom of the slab were fixed during the relaxation process. The short-range forces were calculated as a numerical derivative of the total energy.

**Received 12 August; accepted 4 December 2006.**


1. Eigler, D. M. & Schweizer, E. K. Positioning single atoms with a scanning tunnelling microscope. *Nature* **344,** 524–526 (1990).
2. Sugimoto, Y. *et al.* Atom inlays performed at room temperature using atomic force microscopy. *Nature Mater.* **4,** 156–159 (2005).
3. Stipe, B. C., Rezaei, M. A. & Ho, W. Single-molecule vibrational spectroscopy and microscopy. *Science* **280,** 1732–1735 (1998).
4. Heinrich, A. J., Lutz, C. P., Gupta, J. A. & Eigler, D. M. Molecule cascades. *Science* **298,** 1381–1387 (2002).
5. Pascual, J. I., Lorente, N., Song, Z., Conrad, H. & Rust, H.-P. Selectivity in vibrationally mediated single-molecule chemistry. *Nature* **423,** 525–528 (2003).
6. Madhavan, V., Chen, W., Jamneala, T., Crommie, M. F. & Wingreen, N. S. Tunneling into a single magnetic atom: spectroscopic evidence of the Kondo resonance. *Science* **280,** 567–569 (1998).
7. Li, J., Schneider, W.-D., Berndt, R. & Delley, B. Kondo scattering observed at a single magnetic impurity. *Phys. Rev. Lett.* **80,** 2893–2896 (1998).
8. Morita, S., Wiesendanger, R. & Meyer, E. *Noncontact Atomic Force Microscopy*. *NanoScience and Technology* (Springer, Berlin, 2002).
9. García, R. & Pérez, R. Dynamic atomic force microscopy methods. *Surf. Sci. Rep.* **47,** 197–301 (2002).
10. Giessibl, F. J. Advances in atomic force microscopy. *Rev. Mod. Phys.* **75,** 949–983 (2003).
11. Lantz, M. A. *et al.* Quantitative measurement of short-range chemical bonding forces. *Science* **291,** 2580–2583 (2001).
12. Abe, M., Sugimoto, Y., Custance, O. & Morita, S. Room-temperature reproducible spatial force spectroscopy using atom-tracking technique. *Appl. Phys. Lett.* **87,** 173503 (2005).
13. Hoffmann, R., Kantorovich, L. N., Baratoff, A., Hug, H. J. & Güntherodt, H.-J. Sublattice identification in scanning force microscopy on alkali halide surfaces. *Phys. Rev. Lett.* **92,** 146103 (2004).
14. Pérez, R., Payne, M., Štich, I. & Terakura, K. Role of covalent tip-surface interactions in noncontact atomic force microscopy. *Phys. Rev. Lett.* **78,** 678–681 (1997).
15. Livshits, A. I., Shluger, A. L., Rohl, A. L. & Foster, A. S. Model of noncontact scanning force microscopy on ionic surfaces. *Phys. Rev. B* **59,** 2436–2448 (1999).
16. Abe, M., Sugimoto, Y., Custance, O. & Morita, S. Atom tracking for reproducible force spectroscopy at room temperature with non-contact atomic force microscopy. *Nanotechnology* **16,** 3029–3034 (2005).
17. Oyabu, N. *et al.* Single atomic contact adhesion and dissipation in dynamic force microscopy. *Phys. Rev. Lett.* **96,** 106101 (2006).
18. Ke, S. H., Uda, T., Pérez, R., Štich, I. & Terakura, K. First-principles investigation of tip-surface interaction on a GaAs(110) surface: implications for atomic force and scanning tunneling microscopies. *Phys. Rev. B* **60,** 11631–11638 (1999).
19. Hembacher, S., Giessibl, F. J. & Mannhart, J. Force microscopy with light-atom probes. *Science* **305,** 380–383 (2004).
20. Sugimoto, Y. *et al.* Real topography, atomic relaxations, and short-range chemical interactions in atomic force microscopy: The case of the α-Sn/Si(111)-$(\sqrt{3} \times \sqrt{3})$R30° surface. *Phys. Rev. B* **73,** 205329 (2006).
21. Sugimoto, Y. *et al.* Non-contact atomic force microscopy study of the Sn/Si(111) mosaic phase. *Appl. Surf. Sci.* **241,** 23–27 (2005).
22. Charrier, A. *et al.* Contrasted electronic properties of Sn-adatom-based $(\sqrt{3} \times \sqrt{3})$R30° reconstructions on Si(111). *Phys. Rev. B* **64,** 115407 (2001).
23. Albrecht, T. R., Grütter, P., Horne, D. & Rugar, D. Frequency modulation detection using high-Q cantilevers for enhanced force microscope sensitivity. *J. Appl. Phys.* **69,** 668–673 (1991).
24. Giessibl, F. J. Forces and frequency shifts in atomic resolution dynamic-force microscopy. *Phys. Rev. B* **56,** 16010–16015 (1997).
25. Sader, J. E. & Jarvis, S. P. Accurate formulas for interaction force and energy in frequency modulation force spectroscopy. *Appl. Phys. Lett.* **84,** 1801–1803 (2004).
26. Jelinek, P., Wang, H., Lewis, J. P., Sankey, O. F. & Ortega, J. Multicenter approach to the exchange-correlation interactions in ab initio tight-binding methods. *Phys. Rev. B* **71,** 235101 (2005).


**Supplementary Information** is linked to the online version of the paper at www.nature.com/nature.

**Acknowledgements** We thank F. J. Giessibl and M. Reichling for their comments on the manuscript, and T. Namikawa and K. Mizuta for technical assistance. This work was supported by the Handai FRC, the JST, the 21st Century COE programme, and the MEXT of Japan. The work of P.P. and R.P. is supported by the MCyT, the Juan de la Cierva Programme, the CCC-UAM (Spain), and the FORCETOOL project (EU). The work of P.J. is supported by the MSMT and GAAV.

**Author Information** Reprints and permissions information is available at www.nature.com/reprints. The authors declare no competing financial interests. Correspondence and requests for materials should be addressed to O.C. (oscar@afm.eei.eng.osaka-u.ac.jp).